JOURNAL OF GEOPHYSICAL RESEARCH, VOL. 99, NO. B4, PAGES 7045–7055, APRIL 10, 1994

Mechanics of wedge-shaped fault blocks 2. An elastic solution for extensional wedges

An Yin

Department of Earth and Space Sciences, University of California, Los Angeles

Abstract. Listric, planar, low-angle, and high-angle normal faults are common in hanging walls of detachment faults. An elastic model has been developed to evaluate the role of basal friction, wedge geometry, pore fluid pressure within the wedge, and boundary conditions applied along the wedge rear in controlling the stress distribution in an extensional fault wedge. This model assumes a stress-free condition on the top and frictional sliding on the base of the wedge, respectively, a linear variation of stress components as a function of depth along the wedge rear, and a uniform horizontal stress applied on the wedge toe. The model predicts that (1) for the surface slope equal to zero, a thin wedge favors development of high-angle and planar faults, whereas a thick wedge favors development of low-angle and listric normal faults; variation of pore fluid pressures along the basal detachment fault hardly affects the predicted fault geometry; pore fluid pressure within the wedge is critical in controlling the state of stress in the wedge: higher values of the internal pore fluid pressure promote low-angle normal faulting and locally high-angle reverse faulting; (2) variation of surface slope and the uniform horizontal normal stress applied at the wedge toe does not affect the predicted fault geometry appreciably, although the distribution of deviatoric stress magnitude changes for different cases; and (3) listric normal faults are predicted in all computations and the fault curvature increases as the vertical gradient of the horizontal normal stress along the wedge rear, the wedge angle (surface slope + dip angle), and the internal pore fluid pressure increase. The model provides a simple conceptual guide to deciphering the formation of complex fault geometries and cross cutting relationships as a function of mechanical parameters related to geologic processes and settings. For example, it provides an explanation for why low-angle normal faults cut high-angle normal faults in hanging walls of some detachment fault systems in the U.S. Cordillera.

Introduction

Low-angle normal faults of regional extent (detachment faults) are dominant structures in extensional terranes [e.g., *Wernicke*, 1981; *Lister and Davis*, 1989]. Intense geologic investigations of low-angle normal fault systems in western United States and elsewhere in the world in the last two decades have greatly enhanced our understanding of their geometries and kinematics [e.g., *Gibbs*, 1984; *Lister et al.*, 1986; *Morley*, 1989; *Tulloch and Kimbrough*, 1989; *Wernicke*, 1993; *Dinter and Royden*, 1993]. However, mechanical conditions for the initiation and the development of low-angle normal fault sytems remain poorly understood. There are three fundmental problems regarding their mechanics. First, the directions of principal stresses are commonly assumed to be horizontal and vertical during extension, and thus normal faults should initiate at a dip of about 60^0 as predicted by the *Anderson* [1942] theory. If so, why do low-angle normal faults initiate as observed in the field [e.g., *Wernicke*, 1993]? Second, translation of a large rock mass along a low-angle surface requires an extremely low friction on the surface [*Hubbert and Rubey*, 1959], what are the mechanisms that caused friction reduction? Third, once a throughgoing master detachment fault forms and begins to move, what is the state of stress in its hanging wall and how does stress distribution vary as a function of basal friction, wedge geometry, and boundary conditions applied on the wedge rear and the wedge toe? The first question has been addressed by *Yin* [1989, 1990]. He attributed the initiation of low-angle normal faults to a combination of shearing on the base of the upper crust that rotates the stress orientation [*Yin*, 1989] and the presence of high pore fluid pressure that weakens the upper crust [*Yin*, 1990]. *Yin* [1993] also suggested that low-angle normal faults can initiate in a compressional wedge when the friction is high along the basal thrust. Initiation of low-angle normal faults is thought to be related to either upward warping of the Moho [*Spencer and Chase*, 1989] or relaxation of the upper crust behaving viscoelastically and being sheared at its base [*Melosh*, 1990].

The second problem of why motion can occur along low-angle detachment faults is discussed by *Forsyth* [1992], *Axen* [1992], and *Xiao et al.* [1991]. Forsyth investigated the force balance between the regional stress, friction along a normal fault, and stress induced by lithospheric flexure caused by slip along the normal fault. He suggested that motion along low-angle normal faults is favored. *Axen* [1992] reviewed geologic features in detachment fault zones that may indicate the presence of high pore fluid pressures during their development. Low friction induced by high pore fluid pressures in the detachment fault zones may have facilitated motion along low-angle normal faults. The stability of extensional wedges moving along low-angle normal faults

Paper number 93JB02389.
0148-0227/94/93JB-02389$05.00

was also discussed by *Xiao et al.* [1991], who assumed that the wedges deform following the Coulomb fracture criterion. They demonstrated that wedges narrower than the critical-Coulomb-wedge geometry can slide stably along detachment faults without internal deformation.

Geologic studies in the last two decades have revealed complex fault geometries and cross cutting relationsips in hanging walls of detachment faults [e.g., *Anderson*, 1971; *Proffett*, 1977; *Wernicke and Burchfiel*, 1982; *Gibbs*, 1983; *Miller et al.*, 1983; *Lister and Davis*, 1989; *Yin and Dunn*, 1992], suggesting that the state of stress is complex. For example, in some extensional terranes, high-angle normal faults consistently cut low-angle normal faults [e.g., *Proffett*, 1977], whereas in others, low-angle faults cut high-angle faults [e.g., *Lister and Davis*, 1989]. Thus understanding the factors that control the state of stress in detachment fault hanging walls is a key to deciphering the causes for the observed variability in fault geometries and fault kinematics.

Because the geometry of detachment fault hanging walls is approximately wedge-shaped, an elastic wedge model has been developed in this paper. The model relates the stress distribution in an extensional wedge to the basal friction, the wedge geometry, the wedge length, and the boundary conditions applied on the wedge rear and the wedge toe. The formulation of this model is similar to that of the compressional wedge model developed by *Yin* [1993] except that the slip along the basal-bounding fault is in the opposite sense. A simple elastic wedge model was developed earlier by *Spencer* [1982] to inveistigate the stress distribution in hangingwalls of detachment faults. However, his model neglects frictional traction along detachment faults and pore-fluid pressures in the wedge, and thus it is unable to evaluate how pore fluid pressure ratios within and along the base of the wedge affect the state of stress in extensional wedges.

Detachment faults are commonly domal and basinal due to isostatic rebound or constrictional strain field [e.g., *Yin*, 1991]. The model developed below neglects mechanisms and processes for the formation of domal and basinal geometries. Thus it applies to planar detachment faults or early stages of their development when their geometries were planar.

Theory

The geometry of an elastic-brittle extensional wedge and the framework of reference used in the calculations are shown in Figure 1, where α is the surface slope, β is the dip angle of the basal detachment fault, $\theta = \alpha + \beta$, and x_0 is the prescribed wedge length. Note that the x axis is parallel to the surface and points in the upslope direction. The sign convention follows that of elasticity, i.e., tensile stress is positive.

The stress equilibrium equations of a porous continuum in the x and y directions for a plane stress condition are

$$\frac{\partial \overline{\sigma}_{xx}}{\partial x} + \frac{\partial \sigma_{xy}}{\partial y} + X_e = 0 \tag{1}$$

$$\frac{\partial \sigma_{xy}}{\partial x} + \frac{\partial \overline{\sigma}_{yy}}{\partial y} + Y_e = 0 \tag{2}$$

where

$$X_e = -(1-\lambda)\rho_s g \sin\alpha = -\rho_e g \sin\alpha \tag{3}$$

$$Y_e = (1-\lambda)\rho_s g \cos\alpha = \rho_e g \cos\alpha \tag{4}$$

and ρ_s is the average density of rock composing the wedge, λ is the pore fluid pressure ratio within the wedge, g is the acceleration of gravity, $\rho_e = (1-\lambda)\rho_s$ is the effective density, $\overline{\sigma}_{xx}$ and $\overline{\sigma}_{yy}$ are effective normal stress components, and $\sigma_{xy} = \sigma_{yx}$ are the shear stress components in the x and y directions.

The boundary conditions are a stress-free upper surface and a linear variation of normal and shear tractions with depth along the wedge rear, i.e.,

$$\overline{\sigma}_{yy}(x,0) = \sigma_{xy}(x,0) = 0 \tag{5}$$

$$\overline{\sigma}_{xx}(x_0,y) = A + By \tag{6}$$

$$\sigma_{xy}(x_0,y) = Cy \tag{7}$$

where A, B, and C are prescribed constants that define the boundary condition. This assumed boundary condition along the wedge rear is based on in situ stress measurements [*McGarr and Gay*, 1978] which suggests that vertical and horizontal normal stresses are generally a linear function of depth. The boundary condition along the base of the wedge is assumed to follow Amonton's law [*Jaeger and Cook*, 1979]

$$\tau_b(x, y = x\tan\theta) = \mu_b(1-\lambda_b)\overline{\sigma}_b(x, y = x\tan\theta) \tag{8}$$

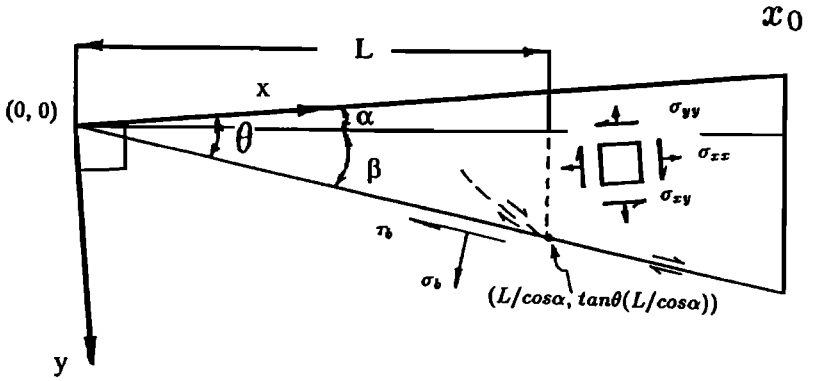

Figure 1. Framework of reference and sign convention used in the model. L, critical length of unfractured wedge toe; α, surface slope; β, dip of the detachment fault bounding the base of the wedge; and $\theta = \alpha + \beta$, wedge angle.

where μ_b is the coefficient of friction along the fault plane, $\overline{\sigma}_b$ is the normal stress component across the basal thrust plane, τ_b is the shear stress component along the basal detachment fault plane, and λ_b is the pore fluid pressure ratio along the fault plane. $\overline{\sigma}_b$ and τ_b can be related to stress components $\overline{\sigma}_{xx}$, $\overline{\sigma}_{yy}$, and σ_{xy} along the basal plane by

$$\overline{\sigma}_b = l^2\overline{\sigma}_{xx} + m^2\overline{\sigma}_{yy} + 2lm\sigma_{xy} \tag{9}$$

$$\tau_b = \sigma_{xy}(l^2 - m^2) + (\overline{\sigma}_{yy} - \overline{\sigma}_{xx})lm \tag{10}$$

where $l = -\sin\theta$ and $m = \cos\theta$.

I have obtained a solution of the above problem by assuming that the Airy stress function has the form

$$\Phi = \frac{1}{6}k_1x^3 + \frac{1}{2}k_2x^2y + \frac{1}{2}k_3xy^2 + \frac{1}{6}k_4y^3 + \frac{1}{6}k_5xy^3 + \frac{1}{2}k_6x^3y + \frac{1}{2}k_7x^2 + \frac{1}{2}k_8y^2 \tag{11}$$

where Φ satisfies the biharmonic equation $\nabla^4\Phi = 0$. This gives

$$\overline{\sigma}_{xx} = \frac{\partial^2\Phi}{\partial y^2} - X_e x = k_3x + k_4y + k_5xy + k_8 + \rho_e g x\sin\alpha \tag{12}$$

$$\overline{\sigma}_{yy} = \frac{\partial^2\Phi}{\partial x^2} - Y_e y = k_1x + k_2y + k_6xy + k_7 - \rho_e g y\cos\alpha \tag{13}$$

$$\sigma_{xy} = -\frac{\partial^2\Phi}{\partial x\partial y} = -k_2x - k_3y - \frac{1}{2}k_5y^2 - \frac{1}{2}k_6x^2 \tag{14}$$

where k_1 to k_8 are constants, their values being determined to fit the boundary conditions. Equation (5) requires that $k_1 = k_2 = k_6 = k_7 = 0$. The remaining constants k_3, k_4, k_5, and k_8 are determined by the following constraints. First, the stress magnitude at the toe of the extensional wedge is assumed to be known, giving

$$\overline{\sigma}_{xx}(0,0) = k_8 = \sigma_0. \tag{15}$$

This condition is equivalent to a uniform normal stress σ_0 in the x direction applied throughout the wedge. Constant k_5 represents the gradient of $\partial\overline{\sigma}_{xx}/\partial y$ in the x direction. Because this gradient varies little in a large region shown by the result of in situ stress measurements [*McGarr and Gay, 1978*], k_5 is assumed to be zero. Finally, k_3 can be determined by (8), (9), and (10) as a function of k_4 and k_8

$$k_3 = \frac{-k_4a_{12} + b_1}{a_{11}} \tag{16}$$

where

$$a_{11} = x_0[\sin 2\theta - \tan\theta\sin^2\theta - \mu_b(1-\lambda_b)\sin^2\theta] \tag{17}$$

$$a_{12} = x_0\sin^2\theta[1 - \tan\theta\mu_b(1-\lambda_b)] \tag{18}$$

$$b_1 = \rho_e g x_0\sin\theta[(\sin\alpha\cos\theta + \cos\alpha\sin\theta) - \mu_b(1-\lambda)(\sin\alpha\sin\theta - \cos\alpha\cos\alpha)] + k_8\sin\theta[\cos\theta - \mu_b(1-\lambda)\sin\theta] \tag{19}$$

and x_0 is the length of the extensional wedge.

We can now write the stress distribution in the wedge as

$$\overline{\sigma}_{xx} = k_3x + k_4y + k_8 + \rho_e g x\sin\alpha \tag{20}$$

$$\overline{\sigma}_{yy} = -\rho_e g y\cos\alpha \tag{21}$$

$$\sigma_{xy} = -k_3y. \tag{22}$$

From (16), (17), and (18), we can see that if $k_8 = 0$, then determination of k_3 is independent of the prescribed wedge length, x_0. In this special case, the solution of stress distribution represented by (20), (21), and (22) is self-similar.

Using the boundary conditions along the wedge rear represented by (6) and (7) and comparing them with (20) and (22), we obtain the following relations:

$$\overline{\sigma}_{xx}(x_0, y) = A + By = k_3x_0 + k_4y + k_8 + \rho_e g x_0\sin\alpha \tag{23}$$

$$\sigma_{xy}(x_0, y) = Cy = -k_3y \tag{24}$$

where $A = k_3x_o + \rho_e g x_o sin\alpha + k_8$, $B = k_4$, and $C = -k_3$. By observing that k_3 is a function of k_4 in (16), we find that B and C are related. Thus, prescribing the value of k_4 and k_8 is equivalent to knowing the boundary conditions (i.e., the value of A and B) at the wedge rear. Parameter $B = k_4$ represents the gradient of $\overline{\sigma}_{xx}$ in the y direction along the wedge rear.

Equation (8) provides the constraint on the shear traction on the basal surface. As k_3, k_4, and k_8 are known, the normal traction along this surface can also be derived from (9)

$$\overline{\sigma}_b(x, y = x\tan\theta) = l^2(k_3x + k_4x\tan\theta + k_8 + \rho_e g x\sin\alpha) + m^2(-\rho_e g x\tan\theta\cos\alpha) + 2lm(-k_3x\tan\theta). \tag{25}$$

Thus, equations (5), (6), (7), (8), and (25) provide a complete set of boundary conditions around an extensional wedge.

Using (20), (21), and (22), the principal stress directions and the maximum shear stress (=deviatoric stress) can be calculated by

$$\psi = \frac{1}{2}\tan^{-1}\left(\frac{2\sigma_{xy}}{\overline{\sigma}_{xx} - \overline{\sigma}_{yy}}\right) \tag{26}$$

and

$$\tau_{max} = \sqrt{\frac{1}{4}(\overline{\sigma}_{xx} - \overline{\sigma}_{yy})^2 + \sigma_{xy}^2} \tag{27}$$

respectively, where ψ is the angle between the maximum tensile stress $\overline{\sigma}_1$ and the x axis. Using (26) and (27), and applying the Coulomb fracture criterion with the assumption that an angle of internal friction ϕ of 30^0, the trajectories of predicted fault patterns and distribution of the maximum shear stress can be calculated.

Results

Using the elastic solution for extensional wedges derived above, the roles of wedge geometry, basal friction, internal pore fluid pressure, wedge length, and boundary conditions

applied on the wedge rear and toe in controlling the state of stress are evaluated. Figure 2 shows the distribution of deviatoric stress and the predicted fault pattern as a function of wedge geometry for $k_8 = 10$ bars, $k_4 = -0.8\rho g$, $\lambda = \lambda_b = 0.4$, and $x_0 = 50$ km. For $\alpha = 0^0$ and $\beta = 10^0$, nearly planar normal faults are predicted (Figure 2*a*). If the surface slope α remains as zero, but the dip angle β increases to 20^0 (Figure 2*b*), the normal faults predicted are more curved (cf. Figure 2*a*). If the surface slope decreases to $\alpha = -3^0$ and the dip angle remains the same as $\beta = 20^0$, the predicted fault pattern (Figure 2*c*) does not change appreciably from that shown in Figure 2*b*. However, if the surface slope increases, the predicted normal faults are less curved and dip at shallower angles (Figure 2*d*) compared to those in Figure 2b. For a detachment fault with its dip angle $\beta = 45^0$ (Figure 2*e*), the predicted normal faults are high-angle in the upper part of the wedge and low-angle in the lower part of the wedge. The distribution of the deviatoric stress in this case is quite different from that shown in Figure 2*b*.

Because the stress solution represented by (20), (21), and (22) is self-similar for $k_8 = 0$, the predicted fault pattern for extensional wedges with various lengths should be the same, although the maximum magnitude of deviatoric stress in these wedges may change. Figures 3*a*, 3*b* and 3*c* show distributions of deviatoric stress and predicted fault patterns for wedge length of $x_0 = 10$ km, 50 km, and 100 km, respectively. Other parameters are chosen to be $k_8 = 0$ bars, $k_4 = -0.8\rho g$, $\alpha = 0^0$, $\beta = 20^0$, and $\lambda = \lambda_b = 0.4$. We can see that the predicted geometries of fault pattern for the three cases are identical. However, as the wedge length increases, the maximum value of deviatoric stress in the wedge increases drastically.

The role of pore fluid pressures within and along the base of an extensional wedge is examined. Figure 4*a* shows the distribution of deviatoric stress and the predicted fault pattern for $k_8 = 10$ bars, $k_4 = -0.8\rho g$, $\lambda = 0.4$, $\lambda_b = 0.9$, $x_0 = 50$ km, $\alpha = 0^0$, and $\beta = 20^0$. Although $\lambda_b = 0.9$ in Figure 4a is much greater than $\lambda_b = 0.4$ in Figure 2b, the predicted fault patterns are quite similar for the two situations. However, the maximum value of deviatoric stress increases as the basal pore fluid pressure ratio decreases. When λ_b and λ increase to 0.9 (Figure 4*b*), both the maximum value of deviatoric stress and the fault pattern change dramatically compared to those in Figures 4a and 2b. In this case, listric and low-angle planar normal faults are predicted. If the basal pore fluid pressure ratio decreases from λ_b=0.9 to λ_b=0.4 but the pore fluid pressure ratio in the

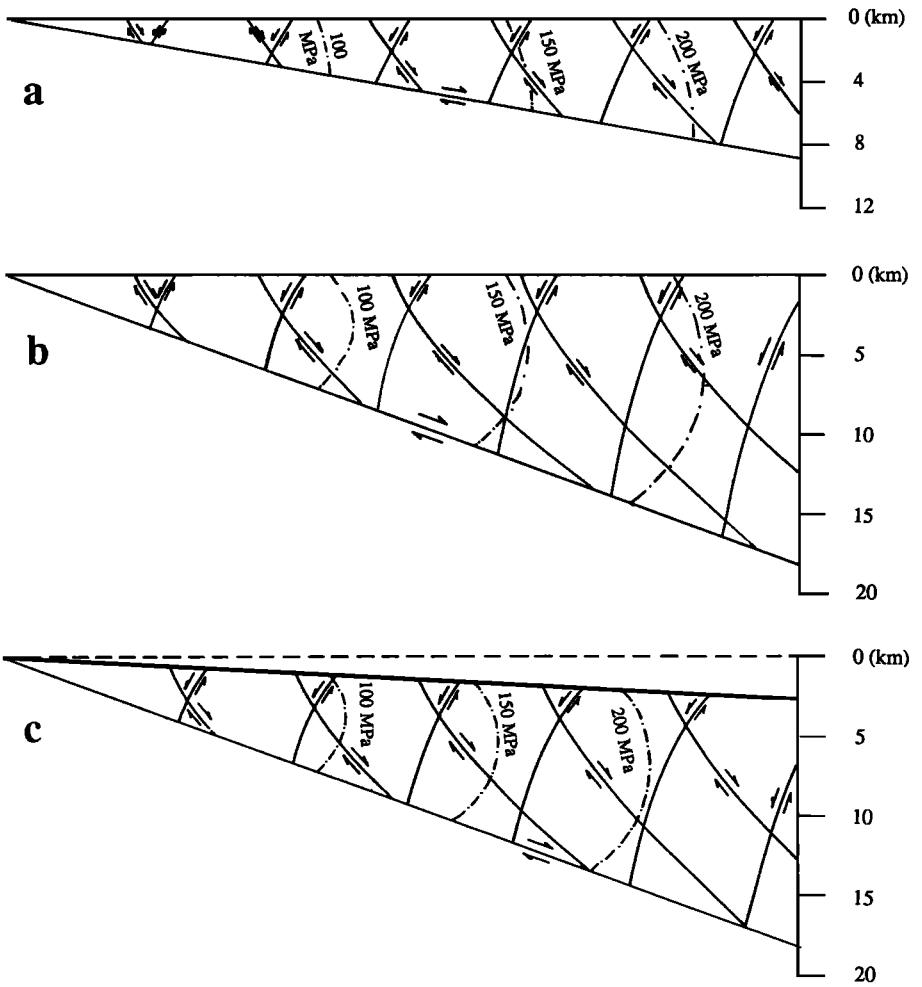

Figure 2. Distributions of deviatoric stress and predicted fault patterns as a function of wedge geometry. Parameters are chosen to be $k_8 = 10$ bars, $k_4 = -0.8\rho g$, $\lambda = \lambda_b = 0.4$, and $x_0 = 50$ km. (a) $\alpha = 0^0$ and $\beta = 10^0$, (b) $\alpha = 0^0$ and $\beta = 20^0$, (c) $\alpha = -3^0$ and $\beta = 20^0$, (d) $\alpha = 3^0$ and $\beta = 20^0$, and (e) $\alpha = 0^0$ and $\beta = 30^0$.

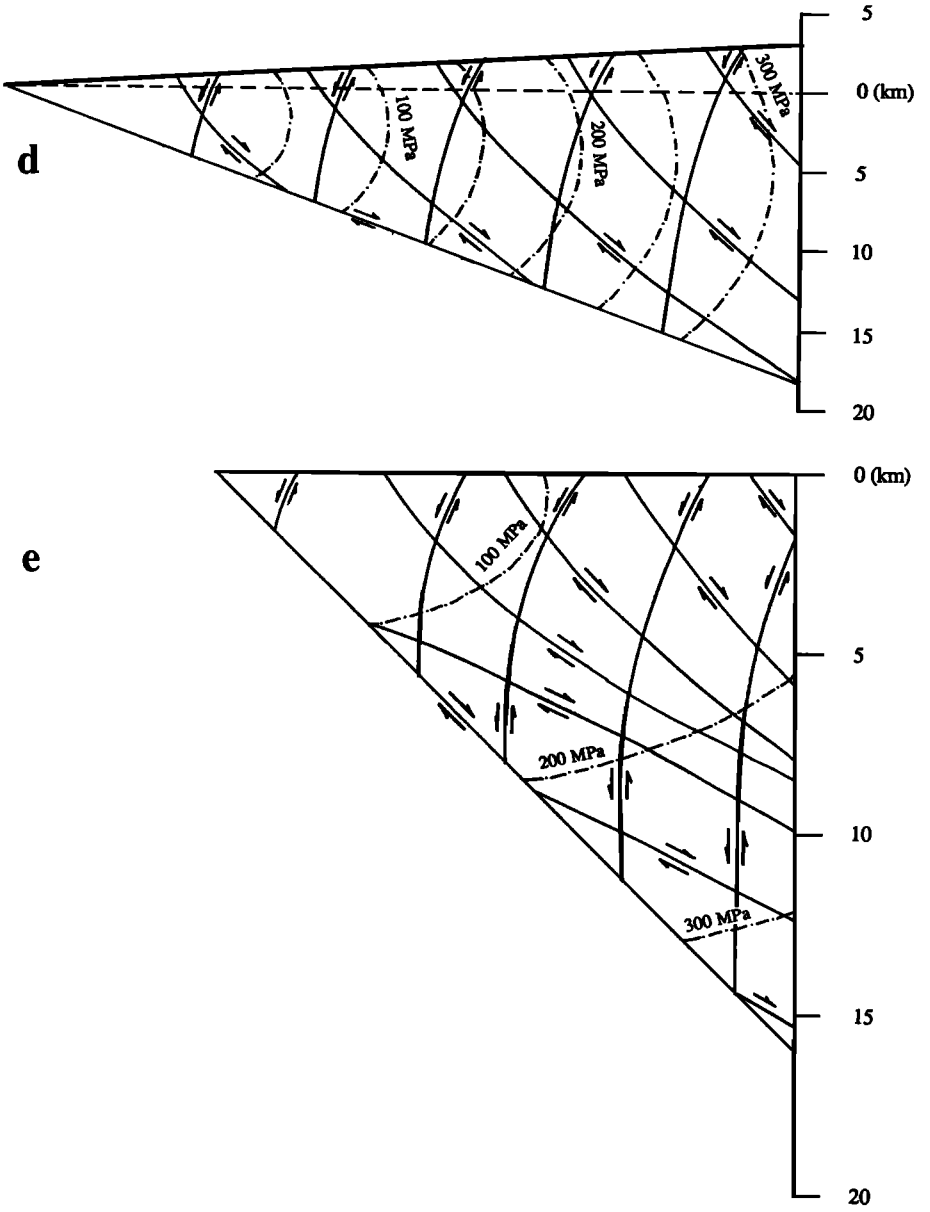

Figure 2. (continued)

wedge remains as high as $\lambda = 0.9$ (Figure 4*c*), we find that the fault pattern is similar to that in Figure 4*b*. However, the maximum value of deviatoric stress in the wedge is less than that in Figure 4*b*.

The role of the normal stress component in the x direction applied on the wedge toe is evaluated in Figure 5. It shows distributions of deviatoric stresses and predicted fault patterns for $k_8 = 30$ bars (Figure 5*a*) and -10 bars (Figure 5*b*), respectively. The rest of the parameters are assumed to be $\alpha = 0^0$, $\beta = 20^0$, $k_4 = -0.9\rho g$, $\lambda = 0.4$, $\lambda_b = 0.9$, and $x_0 = 50$ km. We can see that the fault pattern and the distribution of deviatoric stress in both situations are similar.

The last parameter to be evaluated is k_4, the vertical gradient of the normal stress component in the x direction along the wedge rear. Figure 6 shows distributions of deviatoric stress and predicted fault patterns for $k_4 = -1.3\rho g$ (Figure 6*a*) and $k_4 = -0.5\rho g$ (Figure 6*b*). For both cases, we assume that $\alpha = 0^0$, $\beta = 20^0$, $k_8 = 10$ bars, $\lambda = 0.4$, $\lambda_b = 0.4$, and $x_0 = 50$ km. We find that the curvatures of the predicted normal faults are appreciably different in that the greater value of k_4 (e.g., $k_4 = -0.5\rho g$) favors higher-angle and more planar faults.

Discussion

Curvature of Normal Faults

Listric normal faults are common features in extensional wedges [e.g., *Wernicke and Burchfiel*, 1982; *Gibbs*, 1984]. The results of the simple mechanical model presented above indicate that listric normal faults are generally favored in wedge-shaped hanging walls, although their curvatures can vary depending on the boundary conditions applied. In particular, the wedge geometry, the pore fluid pressure, and the

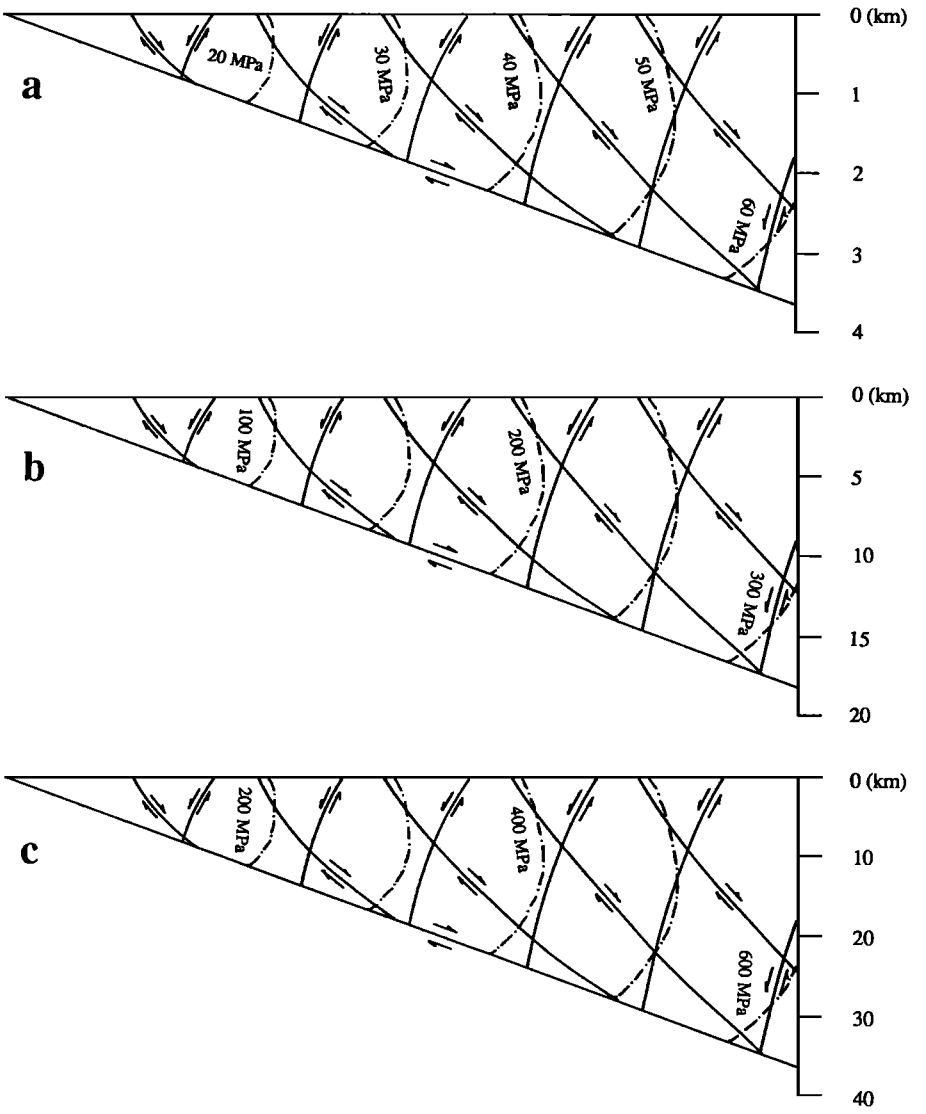

Figure 3. Distributions of deviatoric stress and predicted fault patterns as a function of wedge length. Parameters used in the calculations are $k_8 = 0$ bars, $k_4 = -0.8\rho g$, $\alpha = 0^0$, $\beta = 20^0$, and $\lambda = \lambda_b = 0.4$. (a) $x_0 = 10$ km, (b) $x_0 = 50$ km, and (c) $x_0 = 100$ km.

stress gradient along the wedge rear can all affect the geometry of fault initiation in an extensional wedge. Thin wedges favor the development of high-angle and more planar normal faults, whereas thick wedges favor the development of more curved listric and low-angle normal faults. Although pore fluid pressures along the base of the wedge hardly affect the geometry of potential normal faults in extensional wedges, the pore fluid pressure within extensional wedges is the key factor governing the state of stress in the wedges. Especially, a high pore fluid pressure within the wedge favors the initiation of listric and low-angle normal faults (Figures 4*b* and 4*c*), whereas a low pore fluid pressure within the wedge favors high-angle and more planar normal faults (Figures 2*b* and 4*a*). Because the boundary conditions and wedge geometries can vary among extensional terranes, occurrence of complex fault geometries should be expected as illustrated by the model discussed above. In addition, as the boundary conditions applying to one individual detachment fault system may vary in time during the course of its evolution, faults with different geometries in the hanging wall may cut each other as a result of change in the stress state in response to the change in boundary conditions around the extensional wedge.

Critical Length of an Unfractured Extensional Wedge

A common feature to the results of the above calculations is that the magnitude of deviatoric stress decreases toward the wedge toe. This distribution implies that if normal faults are initiated in an extensional wedge, they should begin to develop first from the wedge rear and then progress toward the wedge toe. This sequence of faulting is excellently demonstrated by *Xiao et al.* [1991] in their sandbox experiments (Figure 7). We can visualize the following sequence of events that may occur during the development of a detachment fault system: (1) a throughgoing detachment fault is initiated, (2) frictional sliding occurs along the

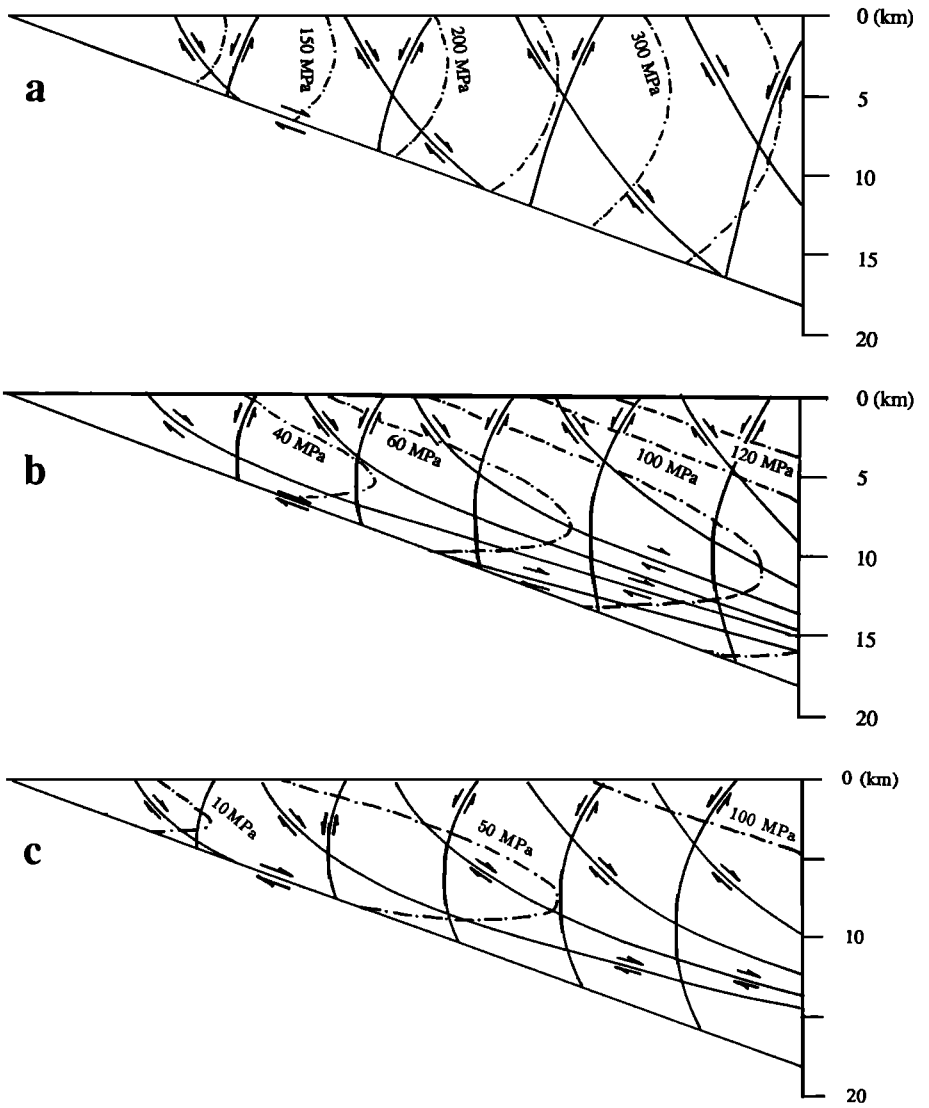

Figure 4. Distributions of deviatoric stress and predicted fault patterns as a function of pore fluid pressure ratios within and along the base of the wedge. Parameters used in the calculations are $k_8 = 10$ bars, $k_4 = -0.8\rho g$, $x_0 = 50$ km, $\alpha = 0^0$, and $\beta = 20^0$. (a) $\lambda = 0.4$ and λ_b=0.9, (b) $\lambda = 0.9$ and λ_b=0.9, (c) $\lambda = 0.9$ and λ_b=0.4.

detachment fault surface, (3) development of hanging wall normal faults begins from the wedge rear, and (4) the size of the unfaulted part of the wedge becomes smaller as the deformational front progresses toward the wedge toe. Finally, there would be a critical wedge length L, where a shorter wedge cannot be further fractured. Determination of this critical length (L) is similar to that of the Hubbert-Rubey toe for compressional wedges as calculated by *Yin* [1993]. Using the same approach, the relation between the critical wedge length (L) and the dip angle of the detachment fault (β) is shown in Figure 8 with $\alpha = 1^0$, λ_b =0.4, $\lambda = 0.4$, $k_8 = 0$, and $k_4 = -0.9\rho g$. The cohesive strength (S_0) is chosen to be 50 bars, 100 bars, and 150 bars, respectively. We find that the critical wedge length decreases monotonically as the dip angle increases. This relationship clearly demonstrates that not only does the strength of the extensional wedge control the length of the unfractured wedge toe, but the configuration of the wedge is also important as well.

Sequence of Normal Fault Development in Extensional Wedges

It has been observed that master detachment faults as well as minor normal faults in their hanging walls can rotate during continental extension [e.g., *Proffett*, 1977]. A consequence of rotating master detachment faults is that the extensional wedge geometry may change in time as detachment fault systems are evolving. Such a change would produce a change in the state of stress in the wedges. For example, shallowing master detachment faults may lead to a change in stress condition from favoring development of listric and low-angle normal faults to one favoring planar and high-angle normal faults, whereas steepening may lead to a change in stress condition from favoring development of more planar and high-angle faults to favoring listric and low-angle normal faults (Figure 2). From the inferences derived from this simple mechanical model, cross cutting relationships between low-angle and high-angle faults observed in

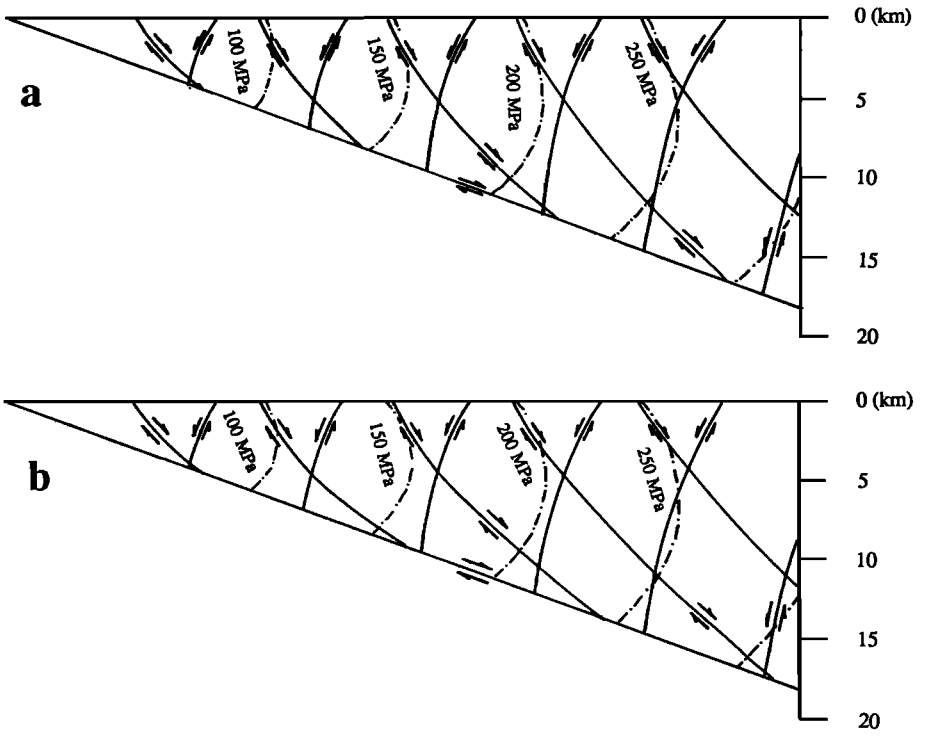

Figure 5. Distributions of deviatoric stress and predicted fault patterns as a function of the normal-traction component in the x direction applied along the wedge rear and the wedge toe. Parameters used in the calculations are $k_4 = -0.8\rho g$, $x_0 = 50$ km, $\lambda = 0.4$, $\lambda_b = 0.9$, $\alpha = 0^0$, and $\beta = 20^0$. (a) $k_8 = 30$ bars, and (b) $k_8 = -10$ bars.

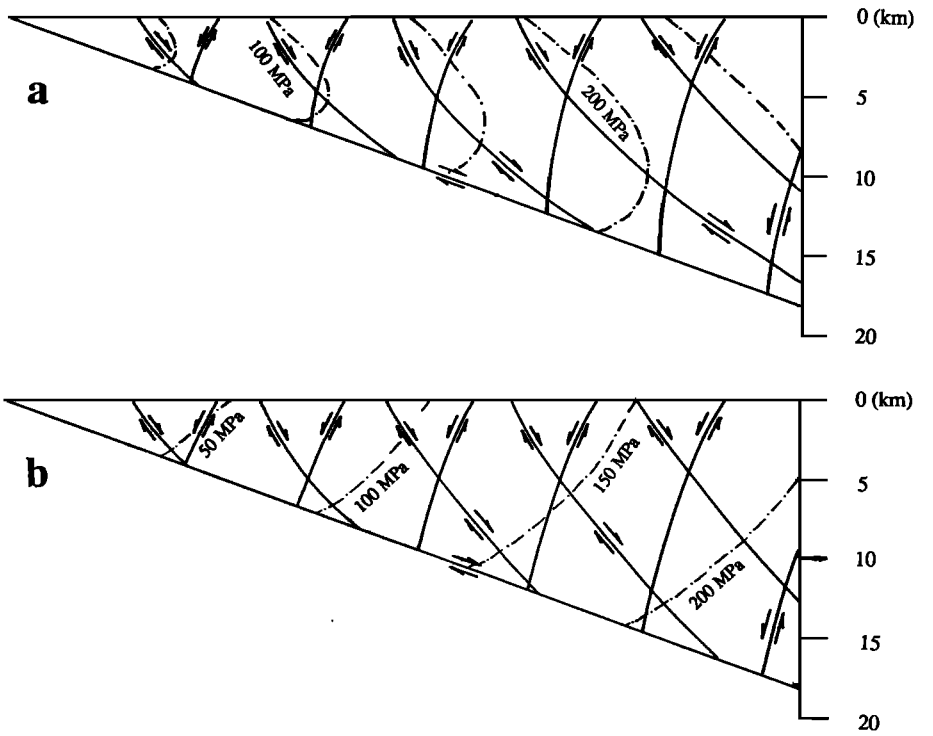

Figure 6. Distributions of deviatoric stress and predicted fault patterns as a function of k_4, the vertical gradient of the normal traction component in the x direction. Parameters used in the calculations are $k_8 = 10$ bars, $x_0 = 50$ km, $\lambda = 0.4$, $\lambda_b = 0.4$, $\alpha = 0^0$, and $\beta = 20^0$. (a) $k_4 = -1.3\rho g$, and (b) $k_4 = -0.5\rho g$.

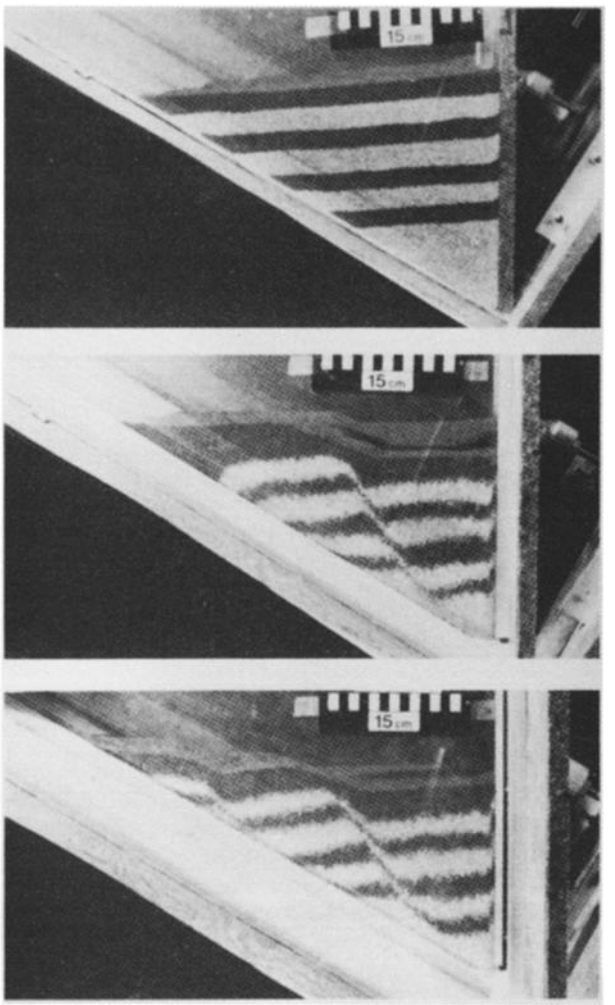

Figure 7. Progressive initiation of normal faults towards the wedge toe in a sandbox experiment for sliding of extensional wedges [*Xiao et al.*, 1991].

hanging walls of detachment faults might indicate whether master detachment faults have shallowed or steepened as they evolved, assuming all other mechanical conditions and parameters remained the same during the change in wedge geometry.

In the Snake Range of eastern Nevada, low-angle normal faults in the hanging wall of the northern Snake Range decollement are consistently cut by high-angle normal faults [*Miller et al.*, 1983]. This type of cross cutting relationship has been explained by rotation of hanging wall high-angle faults to a low-angle orientation mechanically unfavorable for further movement, and thus new high-angle normal faults develop and cut the older rotated normal faults. During this process, the orientations of the principal stresses are assumed to be horizontal and vertical, and initiation of faulting was governed by the Anderson fault theory [*Proffett*, 1977; *Miller et al.*, 1983]. This explanation does not, however, explain the extensional history in the Whipple Mountains detachment fault system, southeastern California where low-angle normal faults excised in the hanging wall truncate an older set of high-angle normal faults [*Lister and Davis*, 1989]. Results of the model presented in this paper may provide a solution to this problem. The Whipple detachment fault itself has not been rotated significantly since its initiation, because the fault cuts at a low angle ($> 30^0$) through the unconformity between the Precambrian basement and Tertiary volcanic and sedimentary strata in its hangingwall (*G.A. Davis*, personal communication, 1989) (also see *Lister and Davis* [1989]). Thus changes in wedge geometry cannot be the cause for the observed cross cutting relationship. Variation in other conditions such as pore fluid pressure in and along the bases of wedges is more likely to cause excisement/initiation of younger low-angle normal faults in the hanging wall of the Whipple detachment fault. For example, the Whipple detachment fault system may have had high pore fluid pressures in the fault zone and low pore fluid pressures in its hanging wall during the early stage of its evolution. This condition would have allowed the development of high-angle normal faults in the hanging wall as shown in Figure 4a. As normal faults in the hanging wall begin to develop, high pore-fluid pressures could be released from the detachment fault zone into the hanging wall. This process may produce a condition of low pore fluid pressures in the detachment fault zone and high pore fluid pressures

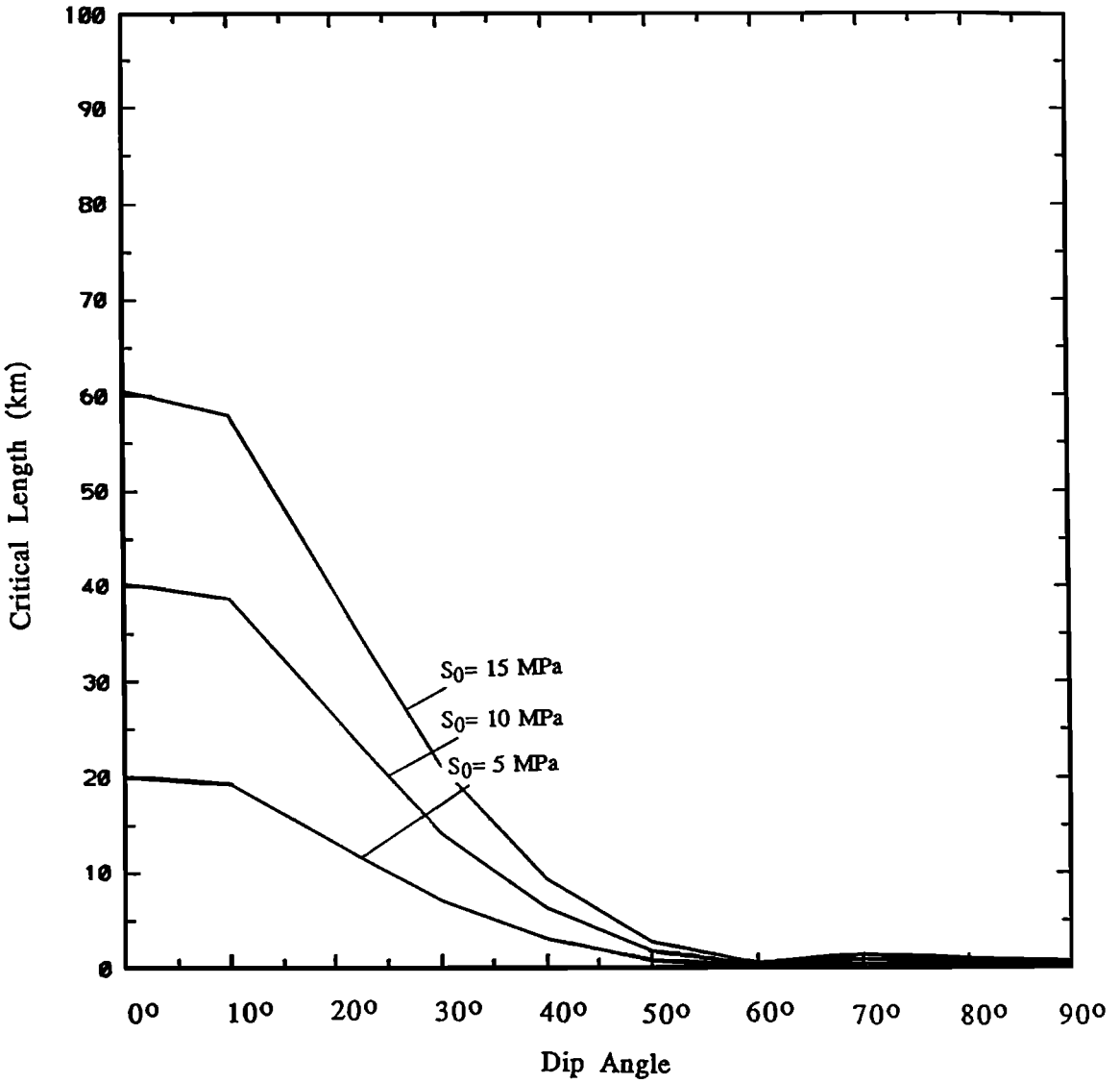

Figure 8. Relationship between the critical length of unfaulted wedge toe and the dip angle of master detachment fault. Parameters used in the calculation are $k_3 = 0$, $k_4 = -0.9\rho g$, $\lambda = 0.4$, $\lambda_b = 0.4$, and $\alpha = 1^0$. S_0 is the cohesive strength of the wedge.

in the wedge-shaped hanging wall. As shown in Figure 4c, this condition would favor the development of both listric and low-angle normal faults.

Alternative to the above explanation for the excisement of low-angle normal faults in the Whipple Mountains, a change in the vertical gradient of the horizontal normal traction along the wedge rear, k_4, may also have caused the change in mode of normal faulting in the hanging wall. It is possible that k_4 was high, say $k_4 = -0.5\rho g$, during the early stage of detachment faulting in the Whipple Mountains. This condition would favor the development of high-angle normal faults as shown in Figure 6a. However, if k_4 decreased as the detachment system was evolving, the boundary condition along the wedge rear could favor the development of more listric and low-angle normal faults as shown in Figure 6*b*.

Limitations of the Model

The model discussed above provides a conceptual guide that may lead to unravelling the complex relationship between boundary condistions and stress distribution in extensional wedges. The major shortcoming of the appproach is that once faults begin to develop in the wedge, new boundaries are created and thus the boundary conditions change. In this case, the wedge is no longer a continuum. Additionally, the assumption that a throughgoing detachment fault must form before the initiation of its hangingwall normal faults is uncertain, because both can develop simultaneously.

Acknowledgments. This research is partially supported by the Academic Senate Research Fund from the University of California. I thank Ray Price, Martin Bott, and an anonymous JGR reviewer for helpful comments.

References

Anderson, E.M., *The Dynamics of Faulting and Dyke Formation with Application to Britain*, 191 pp., Oliver and Boyd, Edinburgh, 1942.

Anderson, R.E., Thin-skin distension in Tertiary rocks of southwestern Nevada, *Geol. Soc. Am. Bull., 82*, 43-58, 1971.

Axen, G.J., Pore pressure, stress increase, and fault weakening in low-angle normal faulting, *J. Geophys. Res., 97*, 8979-8991, 1992.

Dinter, D.A., and L. Royden, Late Cenozoic extension in northeastern Greece: Strymon Valley detachment system and Rhodope metamorphic core complex, *Geology, 21*, 45-48, 1993.

Forsyth, D.W., Finite extension and low-angle normal faulting, *Geology, 20*, 27-30, 1992.

Gibbs, A.D., Balanced cross-section construction from seismic sections in areas of extensional tectonics, *J. Struc. Geol., 5*, 153-160, 1983.

Gibbs, A.D., Structural evolution of extensional basin margins, *J. Geol. Soc. London, 141*, 609-620, 1984.

Lister, G.S., and G.A., Davis, The origin of metamorphic core complexes and detachment faults formed during Tertiary continental extension in the northern Colorado River Region, U.S.A., *J. Struc. Geol., 11*, 65-94, 1989.

Lister, G.S., M.A. Etheridge, and P.A. Symonds, Detachment faulting and the evolution of passive continental margins, *Geology, 14*, 246-250, 1986.

Hubbert, M.K., and W.W. Rubey, Role of fluid pressure in mechanics of overthrust faulting, I, Mechanics of fluid-filled porous solids and its application to overthrust fauting, *Geol. Soc. Am. Bull., 70*, 115-166, 1959.

Jaeger, J.C., and N.G.W. Cook, Fundamentals of Rock Mechanics, 593 pp., Chapman and Hall, London, 1979.

McGarr, A., and N.C. Gay, State of stress in the Earth's crust, *Annu. Rev. Earth Planet. Sci., 6*, 405-436, 1978

Melosh, H. J., Mechanical basis for low-angle normal faulting in the Basin and Range province, *Nature, 343*, 331-335, 1990

Miller, E.L., P.B. Gans, and J. Garing, The Snake Range decollement: An exhumed mid-Tertiary ductile-brittle transition, *Tectonics, 2*, 239-263, 1983.

Morley, C.K., Extension, detachments, and sedimentation in continental rifts (with particular reference to East Africa), *Tectonics, 8*, 1175-1192, 1989.

Proffett, J.M., Jr., Cenozoic geology of the Yerington District, Nevada, and implications for the nature and origin of Basin and Range faulting, *Geol. Soc. Am. Bull., 88*, 247-266, 1977.

Spencer, J.E., Origin of folds of Tertiary low-angle fault surfaces, southeastern California and western Arizona, in *Mesozoic-Cenzooic Tectonic Evolution of the Colorado River Region, California, Arizona, and Nevada* edited by E.G. Frost and D.L. Martin, pp. 123-134, Cordilleran Publishers, San Diego, Calif., 1982.

Spencer, J.E., and C.G. Chase, Role of crustal flexure in initiation of low-angle normal faults and implications for structural evolution of the Basin and Range province, *J. Geophys. Res., 94*, 1765-1775, 1989.

Tulloch, A.J., and D.L. Kimbrough, The Paparoa metamorphic core complex, New Zealand: Cretaceous extension associated with fragmentation of the Pacific margin of Gondwana, *Tectonics, 8*, 1217-1234, 1989.

Wernicke, B., Low-angle normal faults in the Basin and Range province: Nappe tectonics in an expanding orogen, *Nature, 291*, 645-647, 1981.

Wernicke, B., Cenozoic extensional tectonics of the U.S. Cordillera, in *The Geology of North America, vol. G3, The Cordilleran Orogen: Conterminous United States*, edited by B.C. Burchfiel, P.W. Lipman, and M.L. Zoback, Geological Society of America, Boulder, Colo., 553-581, 1993.

Wernicke, B.P., and B.C. Burchfiel, Modes of extensional tectonics, *J. Struc. Geol., 4*, 105-115, 1982.

Xiao, H.-B., F.A. Dahlen, and J. Suppe, Mechanics of extensional wedges, *J. Geophys. Res., 96*, 10,301-10,318, 1991.

Yin, A., Origin of regional, rooted low-angle normal faults: A mechanical model and its tectonic implications, *Tectonics, 8*, 469-482, 1989.

Yin, A., Reply, *Tectonics, 9*, 547-549, 1990.

Yin, A., Mechanisms for the formation of domal and basinal detachment faults: A three-dimensional analysis, *J. Geophys. Res., 96*, 14,577-14,594, 1991.

Yin, A., Mechanics of wedge-shaped fault blocks, 1. An elastic solution for compressional wedges, *J. Geophys. Res., 98*, 14,245-14,256, 1993.

Yin, A., and J.F. Dunn, Structural and stratigraphic development of the Whipple-Chemehuevi detachment fault system, southeastern California: Implications for the geometrical evolution of domal and basinal low-angle normal faults, *Geol. Soc. Am. Bull., 104*, 659-674, 1992.

A. Yin, Department of Earth and Space Sciences, University of California, Los Angeles, CA 90024-1567.

(Received March 5, 1993; revised August 9, 1993; accepted August 19, 1993.)